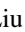




Macroscopic finite-difference scheme based on the mesoscopic regularized lattice-Boltzmann method

Xi Liu ¹, Ying Chen,¹ Zhenhua Chai ^{1,2,3,*} and Baochang Shi ^{1,2,3}

¹*School of Mathematics and Statistics, Huazhong University of Science and Technology, Wuhan 430074, China*

²*Institute of Interdisciplinary Research for Mathematics and Applied Science, Huazhong University of Science and Technology, Wuhan 430074, China*

³*Hubei Key Laboratory of Engineering Modeling and Scientific Computing, Huazhong University of Science and Technology, Wuhan 430074, China*



(Received 30 September 2023; accepted 5 January 2024; published 5 February 2024)

In this paper, we develop a macroscopic finite-difference scheme from the mesoscopic regularized lattice Boltzmann (RLB) method to solve the Navier-Stokes equations (NSEs) and convection-diffusion equation (CDE). Unlike the commonly used RLB method based on the evolution of a set of distribution functions, this macroscopic finite-difference scheme is constructed based on the hydrodynamic variables of NSEs (density, momentum, and strain rate tensor) or macroscopic variables of CDE (concentration and flux), and thus shares low memory requirement and high computational efficiency. Based on an accuracy analysis, it is shown that, the same as the mesoscopic RLB method, the macroscopic finite-difference scheme also has a second-order accuracy in space. In addition, we would like to point out that compared with the RLB method and its equivalent macroscopic numerical scheme, the present macroscopic finite-difference scheme is much simpler and more efficient since it is only a two-level system with macroscopic variables. Finally, we perform some simulations of several benchmark problems, and find that the numerical results are not only in agreement with analytical solutions, but also consistent with the theoretical analysis.

DOI: [10.1103/PhysRevE.109.025301](https://doi.org/10.1103/PhysRevE.109.025301)

I. INTRODUCTION

In the past three decades, the lattice Boltzmann (LB) method, as one of the mesoscopic numerical approaches based on the kinetic models [1–6], has received increasing attention in study of the complex fluid flows, heat, and mass transfer (e.g., the multiphase flows [7], the transport phenomena in porous media [8,9]) governed by the Navier-Stokes equations (NSEs) and convection-diffusion equation (CDE) due to its simplicity in implementation, scalability on parallel computers, extensibility in spatial dimensions, and easy boundary treatment of complex geometries. However, there are some critical problems on this method which are usually mentioned in the published literature [1–6]. The first one is that the LB method may suffer from numerical instability when the relaxation time is close to $1/2$, especially for the popular single-relaxation-time LB (SRT-LB) method [10,11]. To solve this problem, some advanced LB methods are developed, for example, the general multiple-relaxation-time LB (MRT-LB) method [12–14] and the regularized LB (RLB) method [15–17]. In the MRT-LB method, a more general collision term with some free relaxation parameters is introduced such that the classic SRT-LB [10,11] and two-relaxation-time LB (TRT-LB) [18,19] versions can be considered as its two special cases, and the numerical stability can be improved through adjusting these free relaxation parameters [20].

However, how to choose the free relaxation parameters in the MRT-LB method is still an open problem needed to be further considered. In the RLB method, a regularized process is adopted to approximate the nonequilibrium part of the distribution function so that the numerical stability of LB method can be improved [15–17]. Although this approach can be viewed as a special case of the MRT-LB method [14], it is much simpler, and also has the lower memory requirement and data access cost. The second one is that the relation between the mesoscopic LB method and macroscopic partial differential equation based numerical scheme (hereafter named as macroscopic numerical scheme) is still unclear. It should be noted that this problem is not only of great importance in understanding the LB method, but also helpful in analyzing the accuracy and stability of the LB method. For this reason, some works have been performed to obtain the equivalent macroscopic finite-difference schemes of LB methods for the diffusion equations [21–23], the CDEs [24], the Burgers equation [25], and also the NSEs [26–29]. However, these macroscopic numerical schemes based on the LB methods are multiple level in time [26,28], which not only lead to the large memory requirements, but also bring a problem in the implementation of initialization. Actually, there are some special cases that can give the two-level macroscopic numerical schemes. The first case is the SRT-LB method with the relaxation parameter being to unity [30,31], which would lead to a fixed viscosity coefficient for the given lattice spacing and time step. The second case is the macroscopic numerical scheme of the RLB method (M-RLB

*Corresponding author: hustczh@hust.edu.cn

TABLE I. The effect of the relaxation parameter τ_f on numerical results of the present, M-RLB, and RLB schemes for the four-roll mill problem.

	Present	M-RLB	RLB
$\tau_f = 0.7$	6.04×10^{-3}	1.93×10^{-3}	1.93×10^{-3}
$\tau_f = 0.8$	4.02×10^{-3}	2.09×10^{-3}	2.09×10^{-3}
$\tau_f = 1.0$	2.42×10^{-3}	2.42×10^{-3}	2.42×10^{-3}
$\tau_f = 1.2$	1.73×10^{-3}	2.74×10^{-3}	2.74×10^{-3}
$\tau_f = 1.5$	1.21×10^{-3}	3.22×10^{-3}	3.22×10^{-3}

scheme) where a nonconservative variable (a second-order moment of the distribution function for NSEs or a first-order moment of the distribution function for CDE) is introduced [17,32], while how to specify the initial and the boundary conditions of the nonconservative variable is also a problem. The third case is the simplified LB (SLB) method in which the Chapman-Enskog expansion is adopted to give an approximation of the nonequilibrium distribution function [33,34], and the main difference between the SLB method and M-RLB scheme is that different approximations have been used to express the nonequilibrium distribution functions. Last but not least, the memory usage of the LB method also limits its applications in practice; this is owing to the fact that compared with the traditional numerical approaches, a set of distribution functions in the LB method must be stored. To overcome the problems mentioned above, in this work, we will focus on the RLB method, and obtain a new two-level macroscopic numerical scheme with a second-order accuracy from the RLB method. This macroscopic finite-difference scheme can enhance the computational performance of the mesoscopic RLB scheme in entailing significant memory saving and computational efficiency for the large-scale simulations.

The rest of the paper is organized as follows. We first present the RLB method for the NSEs and CDE in Sec. II, and followed by the RLB method based efficient macroscopic finite-difference scheme in Sec. III. In Sec. IV, we conduct a theoretical analysis on the macroscopic finite-difference scheme, and in Sec. V we perform some simulations to test the RLB method, M-RLB method and macroscopic finite-difference scheme, and also give a comparison among them. Finally, some conclusion are summarized in Sec. VI.

TABLE II. The comparisons of the memory usage and computational time among the present, M-RLB, and RLB schemes for the four-roll mill problem [$\tilde{\Psi}$ represents the right-hand side of Eq. (18) or (22), $\Psi = \rho, \mathbf{u}$ or $\mathbf{\Pi}_f$].

	Storage variables	Memory usage	Total time
Present	$\rho[NY][NX], u_1[NY][NX], u_2[NY][NX], F_1[NY][NX]$ $\tilde{\rho}[NY][NX], \tilde{u}_1[NY][NX], \tilde{u}_2[NY][NX], F_2[NY][NX]$	34.78%	7.42s
M-RLB	$\rho[NY][NX], u_1[NY][NX], u_2[NY][NX], F_1[NY][NX]$ $\tilde{\rho}[NY][NX], \tilde{u}_1[NY][NX], \tilde{u}_2[NY][NX], F_2[NY][NX]$ $\Pi_{f,xx}[NY][NX], \Pi_{f,xy}[NY][NX], \Pi_{f,yy}[NY][NX]$ $\tilde{\Pi}_{f,xx}[NY][NX], \tilde{\Pi}_{f,xy}[NY][NX], \tilde{\Pi}_{f,yy}[NY][NX]$	60.87%	7.63s
RLB	$g[NY][NX][Q], \tilde{g}[NY][NX][Q], \rho[NY][NX]$ $u_1[NY][NX], u_2[NY][NX], F_1[NY][NX], F_2[NY][NX]$	100%	8.33s

TABLE III. The effect of the relaxation parameter τ_g on numerical results of the present, M-RLB, and RLB schemes for the isotropic two-dimensional CDE.

	Present	M-RLB	RLB
$\tau_g = 0.6$	9.35×10^{-4}	6.76×10^{-4}	6.76×10^{-4}
$\tau_g = 0.8$	3.14×10^{-3}	2.73×10^{-3}	2.73×10^{-3}
$\tau_g = 1.0$	5.34×10^{-3}	5.34×10^{-3}	5.34×10^{-3}
$\tau_g = 1.2$	7.53×10^{-3}	8.52×10^{-3}	8.52×10^{-3}
$\tau_g = 1.8$	1.41×10^{-2}	2.16×10^{-2}	2.16×10^{-2}

II. REGULARIZED LATTICE BOLTZMANN METHOD FOR THE NAVIER-STOKES AND CONVECTION DIFFUSION EQUATIONS

Generally speaking, the fluid flows, heat, and/or mass transfer can be described by the following NSEs and CDE in d -dimensional space:

$$\partial_t \rho + \nabla \cdot (\rho \mathbf{u}) = 0, \quad (1a)$$

$$\partial_t (\rho \mathbf{u}) + \nabla \cdot (\rho \mathbf{u} \mathbf{u}) = -\nabla p + \nabla \cdot [\rho \nu (\nabla \mathbf{u} + \nabla \mathbf{u}^T)] + \mathbf{F}, \quad (1b)$$

$$\partial_t \phi + \nabla \cdot (\phi \mathbf{u}) = \nabla \cdot (D \nabla \phi) + R, \quad (2)$$

where ρ is the fluid density, \mathbf{u} is the velocity, p is the pressure, ν is the kinematic viscosity [35], and \mathbf{F} is an external force. ϕ is a scalar function related to the position \mathbf{x} and time t , D is the diffusion coefficient, and R is the source term.

In the SRT-LB method with the $DdQq$ (q discrete velocities in d -dimensional space, $d = 1 - 3$) lattice model, the semidiscrete evolution equations for Eqs. (1) and (2) can be written as [14]

$$f_i(\mathbf{x} + \mathbf{c}_i \Delta t, t + \Delta t) = f_i(\mathbf{x}, t) - \frac{1}{\tau_f} [f_i(\mathbf{x}, t) - f_i^{eq}(\mathbf{x}, t)] + \Delta t \left[\tilde{F}_i(\mathbf{x}, t) + F_i(\mathbf{x}, t) + \frac{\Delta t}{2} \tilde{D}_i F_i(\mathbf{x}, t) \right], \quad (3a)$$

TABLE IV. The comparisons of the memory usage and computational time among the present, M-RLB, and RLB schemes for the isotropic two-dimensional CDE at $T = 100$ [$\tilde{\Psi}$ represents the right-hand side of Eq. (19) or (23), $\Psi = \phi$ or Π_g].

	Storage variables	Memory usage	Total time
Present	$\phi[NY][NX], \tilde{\phi}[NY][NX]$	10.53%	11.18s
M-RLB	$\phi[NY][NX], \Pi_{g,x}[NY][NX], \Pi_{g,y}[NY][NX]$ $\tilde{\phi}[NY][NX], \tilde{\Pi}_{g,x}[NY][NX], \tilde{\Pi}_{g,y}[NY][NX]$	31.58%	11.44s
RLB	$f[NY][NX][Q], \tilde{f}[NY][NX][Q], \phi[NY][NX]$	100%	12.64s

$$g_i(\mathbf{x} + \mathbf{c}_i \Delta t, t + \Delta t) = g_i(\mathbf{x}, t) - \frac{1}{\tau_g} [g_i(\mathbf{x}, t) - g_i^{eq}(\mathbf{x}, t)] \\ + \Delta t \left[\tilde{G}_i(\mathbf{x}, t) + G_i(\mathbf{x}, t) \right. \\ \left. + \frac{\Delta t}{2} \tilde{D}_i G_i(\mathbf{x}, t) \right], \quad (3b)$$

where $f_i(\mathbf{x}, t)$ and $g_i(\mathbf{x}, t)$ are the distribution functions at position \mathbf{x} and time t along the velocity \mathbf{c}_i , τ_f and τ_g are the relaxation times, and $f_i^{eq}(\mathbf{x}, t)$ and $g_i^{eq}(\mathbf{x}, t)$ are the corresponding equilibrium distribution functions. $F_i(\mathbf{x}, t)$ and $G_i(\mathbf{x}, t)$ are the discrete forces or source terms, and $\tilde{F}_i(\mathbf{x}, t)$ and $\tilde{G}_i(\mathbf{x}, t)$ are the auxiliary distribution functions that can be used to eliminate the additional terms [14]. Δt is the time step, and $\tilde{D}_i = \partial_t + \gamma \mathbf{c}_i \cdot \nabla$ is a differential operator with $\gamma \in \{0, 1\}$. Based on Eq. (3), the evolution processes can be divided into two substeps generally, i.e., collision and propagation,

Collision:

$$\tilde{f}_i(\mathbf{x}, t) = f_i(\mathbf{x}, t) - \frac{1}{\tau_f} [f_i(\mathbf{x}, t) - f_i^{eq}(\mathbf{x}, t)] \\ + \Delta t \left[\tilde{F}_i(\mathbf{x}, t) + F_i(\mathbf{x}, t) + \frac{\Delta t}{2} \tilde{D}_i F_i(\mathbf{x}, t) \right], \quad (4a)$$

$$\tilde{g}_i(\mathbf{x}, t) = g_i(\mathbf{x}, t) - \frac{1}{\tau_g} [g_i(\mathbf{x}, t) - g_i^{eq}(\mathbf{x}, t)] \\ + \Delta t \left[\tilde{G}_i(\mathbf{x}, t) + G_i(\mathbf{x}, t) + \frac{\Delta t}{2} \tilde{D}_i G_i(\mathbf{x}, t) \right]; \quad (4b)$$

TABLE V. The effect of the relaxation parameter on numerical results of the present, M-RLB, and RLB schemes for the thermal Poiseuille flow with $Pr = 0.25$.

		Present	M-RLB	RLB
$\tau_f = 0.8$	Err(u)	3.86×10^{-4}	1.41×10^{-4}	1.41×10^{-4}
	Err(T)	3.22×10^{-6}	3.28×10^{-6}	3.28×10^{-6}
$\tau_f = 0.95$	Err(u)	1.30×10^{-4}	9.37×10^{-5}	9.37×10^{-5}
	Err(T)	4.30×10^{-6}	5.35×10^{-6}	5.35×10^{-6}
$\tau_f = 1.0$	Err(u)	7.81×10^{-5}	7.81×10^{-5}	7.81×10^{-5}
	Err(T)	4.51×10^{-6}	6.03×10^{-6}	6.03×10^{-6}
$\tau_f = 1.05$	Err(u)	3.58×10^{-5}	6.25×10^{-4}	6.25×10^{-4}
	Err(T)	4.68×10^{-6}	6.72×10^{-6}	6.72×10^{-6}
$\tau_f = 1.15$	Err(u)	2.94×10^{-5}	3.12×10^{-5}	3.12×10^{-5}
	Err(T)	4.94×10^{-6}	8.10×10^{-6}	8.10×10^{-6}

Propagation:

$$f_i(\mathbf{x} + \mathbf{c}_i \Delta t, t + \Delta t) = \tilde{f}_i(\mathbf{x}, t), \quad (5a)$$

$$g_i(\mathbf{x} + \mathbf{c}_i \Delta t, t + \Delta t) = \tilde{g}_i(\mathbf{x}, t), \quad (5b)$$

where $\tilde{f}_i(\mathbf{x}, t)$ and $\tilde{g}_i(\mathbf{x}, t)$ are the postcollision distribution functions.

It should be noted that at the diffusive scaling, i.e., $\Delta t \propto \Delta x^2$, there is no need to include the differential operator \tilde{D}_i in Eq. (3), and the evolution equations can be simplified by

$$f_i(\mathbf{x} + \mathbf{c}_i \Delta t, t + \Delta t) = f_i(\mathbf{x}, t) - \frac{1}{\tau_f} [f_i(\mathbf{x}, t) - f_i^{eq}(\mathbf{x}, t)] \\ + \Delta t F_i(\mathbf{x}, t), \quad (6a)$$

$$g_i(\mathbf{x} + \mathbf{c}_i \Delta t, t + \Delta t) = g_i(\mathbf{x}, t) - \frac{1}{\tau_g} [g_i(\mathbf{x}, t) - g_i^{eq}(\mathbf{x}, t)] \\ + \Delta t G_i(\mathbf{x}, t). \quad (6b)$$

For the NSEs, the equilibrium distribution function f_i^{eq} and discrete force term F_i are given by

$$f_i^{eq}(\mathbf{x}, t) = \omega_i \rho \left[1 + \frac{\mathbf{c}_i \cdot \mathbf{u}}{c_s^2} + \frac{\mathbf{u} \mathbf{u} : (\mathbf{c}_i \mathbf{c}_i - c_s^2 \mathbf{I})}{2c_s^4} \right], \quad (7a)$$

$$F_i(\mathbf{x}, t) = \omega_i \frac{\mathbf{c}_i \cdot \mathbf{F}}{c_s^2}. \quad (7b)$$

For the CDE, however, the equilibrium distribution function g_i^{eq} and discrete source term G_i should be given by

$$g_i^{eq}(\mathbf{x}, t) = \omega_i \phi \left(1 + \frac{\mathbf{c}_i \cdot \mathbf{u}}{c_s^2} \right), \quad (8a)$$

$$G_i(\mathbf{x}, t) = \omega_i R. \quad (8b)$$

To improve the numerical stability of the SRT-LB method (6), we now consider the RLB method where a regularization process is adopted to filter out the nonhydrodynamic content of the nonequilibrium part of the distribution function [i.e., $f_i^{neq}(\mathbf{x}, t) = f_i(\mathbf{x}, t) - f_i^{eq}(\mathbf{x}, t)$ and $g_i^{neq}(\mathbf{x}, t) = g_i(\mathbf{x}, t) - g_i^{eq}(\mathbf{x}, t)$] with the Chapman-Enskog analysis [15], and simultaneously, the second-order accuracy can be preserved [32]. For the NSEs, the evolution equation of the RLB method can be written as [15]

$$f_i(\mathbf{x} + \mathbf{c}_i \Delta t, t + \Delta t) \\ = f_i^{eq}(\mathbf{x}, t) + \left(1 - \frac{1}{\tau_f} \right) \frac{\omega_i (\mathbf{c}_i \mathbf{c}_i - c_s^2 \mathbf{I}) : \Pi_f^{neq}}{2c_s^4} \\ + \Delta t F_i(\mathbf{x}, t), \quad (9)$$

where Π_f^{neq} is the second-order moment tensor of nonequilibrium distribution function, and can be expressed as [36–38]

$$\begin{aligned}\Pi_f^{neq} &= \Pi_f - \Pi_f^{eq} = \sum_i \mathbf{c}_i \mathbf{c}_i f_i - \sum_i \mathbf{c}_i \mathbf{c}_i f_i^{eq} \\ &= \sum_i \mathbf{c}_i \mathbf{c}_i (f_i - f_i^{eq}).\end{aligned}\quad (10)$$

However, the evolution equation for the CDE should be written as [17]

$$\begin{aligned}g_i(\mathbf{x} + \mathbf{c}_i \Delta t, t + \Delta t) &= g_i^{eq}(\mathbf{x}, t) + \left(1 - \frac{1}{\tau_g}\right) \frac{\omega_i \mathbf{c}_i \cdot \Pi_g^{neq}}{c_s^2} \\ &\quad + \Delta t G_i(\mathbf{x}, t),\end{aligned}\quad (11)$$

where Π_g^{neq} is the first-order moment of nonequilibrium distribution function, and can be given by [39–41]

$$\Pi_g^{neq} = \Pi_g - \Pi_g^{eq} = \sum_i \mathbf{c}_i g_i - \mathbf{c}_i g_i^{eq} = \sum_i \mathbf{c}_i (g_i - g_i^{eq}).\quad (12)$$

Through some asymptotic analysis methods [4,14], the NSEs and CDE can be recovered from Eqs. (9) and (11) with a second-order accuracy in space and the following relations:

$$v = \left(\tau_f - \frac{1}{2}\right) c_s^2 \Delta t, \quad D = \left(\tau_g - \frac{1}{2}\right) c_s^2 \Delta t. \quad (13)$$

III. MACROSCOPIC SCHEME BASED ON THE REGULARIZED LATTICE BOLTZMANN METHOD

A. Macroscopic numerical scheme

We now focus on the macroscopic numerical scheme of the RLB method, i.e., M-RLB scheme. First, the evolutions of the RLB method for the NSEs and CDE can be rewritten as

$$\begin{aligned}f_i(\mathbf{x} + \mathbf{c}_i \Delta t, t + \Delta t) &= f_i^{eq}(\mathbf{x}, t) + \left(1 - \frac{1}{\tau_f}\right) \frac{\omega_i (\mathbf{c}_i \mathbf{c}_i - c_s^2 \mathbf{I}) : (\Pi_f - \Pi_f^{eq})}{2c_s^4} \\ &\quad + \Delta t F_i(\mathbf{x}, t),\end{aligned}\quad (14)$$

$$\begin{aligned}g_i(\mathbf{x} + \mathbf{c}_i \Delta t, t + \Delta t) &= g_i^{eq}(\mathbf{x}, t) + \left(1 - \frac{1}{\tau_g}\right) \frac{\omega_i \mathbf{c}_i \cdot (\Pi_g - \Pi_g^{eq})}{c_s^2} \\ &\quad + \Delta t G_i(\mathbf{x}, t),\end{aligned}\quad (15)$$

then one can obtain

$$f_i(\mathbf{x}, t + \Delta t) = \left[f_i^{eq} + \left(1 - \frac{1}{\tau_f}\right) \frac{\omega_i (\mathbf{c}_i \mathbf{c}_i - c_s^2 \mathbf{I}) : (\Pi_f - \Pi_f^{eq})}{2c_s^4} + \Delta t F_i \right] (\mathbf{x} - \mathbf{c}_i \Delta t, t), \quad (16)$$

$$g_i(\mathbf{x}, t + \Delta t) = \left[g_i^{eq} + \left(1 - \frac{1}{\tau_g}\right) \frac{\omega_i \mathbf{c}_i \cdot (\Pi_g - \Pi_g^{eq})}{c_s^2} + \Delta t G_i \right] (\mathbf{x} - \mathbf{c}_i \Delta t, t). \quad (17)$$

Through the summations of f_i , $\mathbf{c}_i f_i$, and $\mathbf{c}_i \mathbf{c}_i f_i$ of Eq. (16) over i , one can derive the M-RLB method for the NSEs,

$$\rho(\mathbf{x}, t + \Delta t) = \sum_i \left\{ \left[f_i^{eq} + \left(1 - \frac{1}{\tau_f}\right) \frac{\omega_i (\mathbf{c}_i \mathbf{c}_i - c_s^2 \mathbf{I}) : (\Pi_f - \Pi_f^{eq})}{2c_s^4} + \Delta t F_i \right] (\mathbf{x} - \mathbf{c}_i \Delta t, t) \right\}, \quad (18a)$$

$$\mathbf{u}(\mathbf{x}, t + \Delta t) = \frac{1}{\rho(\mathbf{x}, t + \Delta t)} \sum_i \left\{ \mathbf{c}_i \left[f_i^{eq} + \left(1 - \frac{1}{\tau_f}\right) \frac{\omega_i (\mathbf{c}_i \mathbf{c}_i - c_s^2 \mathbf{I}) : (\Pi_f - \Pi_f^{eq})}{2c_s^4} + \Delta t F_i \right] (\mathbf{x} - \mathbf{c}_i \Delta t, t) \right\}, \quad (18b)$$

$$\Pi_f(\mathbf{x}, t + \Delta t) = \sum_i \left\{ \mathbf{c}_i \mathbf{c}_i \left[f_i^{eq} + \left(1 - \frac{1}{\tau_f}\right) \frac{\omega_i (\mathbf{c}_i \mathbf{c}_i - c_s^2 \mathbf{I}) : (\Pi_f - \Pi_f^{eq})}{2c_s^4} + \Delta t F_i \right] (\mathbf{x} - \mathbf{c}_i \Delta t, t) \right\}, \quad (18c)$$

where no distribution functions are included. Similarly, we can also give the M-RLB scheme for the CDE [17],

$$\phi(\mathbf{x}, t + \Delta t) = \sum_i \left\{ \left[g_i^{eq} + \left(1 - \frac{1}{\tau_g}\right) \frac{\omega_i \mathbf{c}_i \cdot (\Pi_g - \Pi_g^{eq})}{c_s^2} + \Delta t G_i \right] (\mathbf{x} - \mathbf{c}_i \Delta t, t) \right\}, \quad (19a)$$

$$\Pi_g(\mathbf{x}, t + \Delta t) = \sum_i \left\{ \mathbf{c}_i \left[g_i^{eq} + \left(1 - \frac{1}{\tau_g}\right) \frac{\omega_i \mathbf{c}_i \cdot (\Pi_g - \Pi_g^{eq})}{c_s^2} + \Delta t G_i \right] (\mathbf{x} - \mathbf{c}_i \Delta t, t) \right\}. \quad (19b)$$

Here we would like to point out that, theoretically, the macroscopic numerical scheme (18) or (19) should be the same as the RLB method for NSEs or CDE, while compared with the RLB method with the $DdQq$ lattice model, it shares a low memory. For example, for the D2Q9 lattice model usually

adopted for two-dimensional fluid flow problems, there are at least three macroscopic variables [the density ρ and velocity $\mathbf{u} = (u_1, u_2)$] and nine distribution functions needed to be stored in the RLB method, while in the M-RLB scheme (18), only three macroscopic variables [the density ρ and velocity

$\mathbf{u} = (u_1, u_2)$ and three elements of the symmetric second-order tensor $\mathbf{\Pi}_f$ are needed to store. In addition, it should be noted that there are some problems in the macroscopic numerical scheme, for example, how to implement the initialization and how to specify the boundary condition of $\mathbf{\Pi}_{f,g}$ in numerical simulations.

B. Macroscopic finite-difference scheme

To overcome the above problems and reduce the number of the variables stored in the above macroscopic numerical scheme, we will propose a new macroscopic finite-difference

scheme based on the RLB method. Based on the previous works [36–38], one can give an approximation to $\mathbf{\Pi}_f^{neq}$,

$$\mathbf{\Pi}_f^{neq} = \sum_i \mathbf{c}_i \mathbf{c}_i (f_i - f_i^{eq}) \approx -\rho \tau_f c_s^2 \Delta t (\nabla \mathbf{u} + \nabla \mathbf{u}^T), \quad (20)$$

and similarly, we can also obtain the following result [39–41]:

$$\mathbf{\Pi}_g^{neq} = \sum_i \mathbf{c}_i (g_i - g_i^{eq}) \approx -\tau_g c_s^2 \Delta t \nabla \phi. \quad (21)$$

If we insert Eq. (20) into Eq. (18), one can obtain the semidiscrete macroscopic numerical schemes for the density and velocity governed by NSEs,

$$\rho(\mathbf{x}, t + \Delta t) = \sum_i \left\{ \left[f_i^{eq} + \rho(1 - \tau_f) \Delta t \frac{\omega_i (\mathbf{c}_i \mathbf{c}_i - c_s^2 \mathbf{I}) : (\nabla \mathbf{u} + \nabla \mathbf{u}^T)}{2c_s^2} + \Delta t F_i \right] (\mathbf{x} - \mathbf{c}_i \Delta t, t) \right\}, \quad (22a)$$

$$\mathbf{u}(\mathbf{x}, t + \Delta t) = \frac{1}{\rho(\mathbf{x}, t + \Delta t)} \sum_i \left\{ \mathbf{c}_i \left[f_i^{eq} + \rho(1 - \tau_f) \Delta t \frac{\omega_i (\mathbf{c}_i \mathbf{c}_i - c_s^2 \mathbf{I}) : (\nabla \mathbf{u} + \nabla \mathbf{u}^T)}{2c_s^2} + \Delta t F_i \right] (\mathbf{x} - \mathbf{c}_i \Delta t, t) \right\}. \quad (22b)$$

Following a similar way, from Eq. (21) we can also derive semidiscrete macroscopic numerical scheme for the variable ϕ in the CDE,

$$\phi(\mathbf{x}, t + \Delta t) = \sum_i \left\{ \left[g_i^{eq} + (1 - \tau_g) \Delta t \omega_i \mathbf{c}_i \cdot \nabla \phi + \Delta t G_i \right] (\mathbf{x} - \mathbf{c}_i \Delta t, t) \right\}. \quad (23)$$

Then one can obtain the RLB method based macroscopic finite-difference schemes for the NSEs and CDE (see the details in the following section) once the gradient terms in Eqs. (22) and (23) are discretized by the following second-order central scheme [42–44],

$$\nabla \theta = \sum_{k=1}^{2d} \frac{\bar{\omega}_k \mathbf{c}_k \theta(\mathbf{x} + \mathbf{c}_k \Delta t, t)}{c_s^2 \Delta t}, \quad (24)$$

where θ is an arbitrary scalar function, and $\bar{\omega}_k$ is the weigh coefficient corresponding to the $DdQ2d$ or $D2Q(2d + 1)$ lattice model for simplicity. It should be noted that compared with the RLB and M-RLB methods, the new macroscopic finite-difference scheme shares a much lower memory and there is no need to consider and implement the initialization and boundary condition of $\mathbf{\Pi}_{f,g}$.

IV. ACCURACY ANALYSIS OF THE REGULARIZED LATTICE BOLTZMANN METHOD BASED THE MACROSCOPIC FINITE-DIFFERENCE SCHEME

In this section, we will conduct a detailed theoretical analysis on the accuracy of the RLB method based the macroscopic finite-difference schemes (22) and (23) for the NSEs (1) and CDE (2), where the gradient terms in Eqs. (22) and (23) are discretized by the second-order central scheme (24). To this end, the equilibrium distribution functions (7) and (8) for the NSEs and CDE at the diffusive scaling can be rewritten as

$$f_i^{eq}(\mathbf{x}, t) = \bar{f}_i^{eq} + \tilde{f}_i^{eq} + \underbrace{\omega_i \rho \frac{\mathbf{u} \mathbf{u} : (\mathbf{c}_i \mathbf{c}_i - c_s^2 \mathbf{I})}{2c_s^4}}_{O(\Delta x^2)}, \quad (25a)$$

$$\bar{f}_i^{eq} = \omega_i \rho = O(1), \quad \tilde{f}_i^{eq} = \omega_i \rho \frac{\mathbf{c}_i \cdot \mathbf{u}}{c_s^2} = O(\Delta x), \quad (25b)$$

and

$$g_i^{eq}(\mathbf{x}, t) = \bar{g}_i^{eq} + \tilde{g}_i^{eq}, \quad (26a)$$

$$\bar{g}_i^{eq} = \omega_i \phi = O(1), \quad \tilde{g}_i^{eq} = \omega_i \phi \frac{\mathbf{c}_i \cdot \mathbf{u}}{c_s^2} = O(\Delta x). \quad (26b)$$

Based on Eqs. (25) and (26), applying the Taylor expansion to Eqs. (22) and (23) at the position \mathbf{x} and time t yields the following results:

$$\begin{aligned} \rho + \Delta t \partial_t \rho &= \sum_i f_i^{eq} - \Delta t \nabla_\alpha \sum_i c_{i\alpha} f_i^{eq} + \frac{\Delta t^2}{2} \nabla_\alpha \nabla_\beta \sum_i c_{i\alpha} c_{i\beta} (\bar{f}_i^{eq} + \tilde{f}_i^{eq}) \\ &\quad - \frac{\Delta t^3}{2} \nabla_\alpha \nabla_\beta \nabla_\gamma \sum_i c_{i\alpha} c_{i\beta} c_{i\gamma} \bar{f}_i^{eq} + \sum_i \frac{\omega_i (c_{i\alpha} c_{i\beta} - c_s^2 \delta_{\alpha\beta}) (\tau_f - 1) \tilde{\Pi}_{f,\alpha\beta}^{neq}}{2c_s^2} \\ &\quad - \Delta t \nabla_\eta \sum_i c_{i\eta} \frac{\omega_i (c_{i\alpha} c_{i\beta} - c_s^2 \delta_{\alpha\beta}) (\tau_f - 1) \tilde{\Pi}_{f,\alpha\beta}^{neq}}{2c_s^2} + \Delta t \sum_i F_i + O(\Delta x^4), \end{aligned} \quad (27a)$$

$$\begin{aligned} \rho u_\eta + \Delta t \partial_t (\rho u_\eta) &= \sum_i c_{i\eta} f_i^{eq} - \Delta t \nabla_\alpha \sum_i c_{i\alpha} c_{i\eta} f_i^{eq} + \frac{\Delta t^2}{2} \nabla_\alpha \nabla_\beta \sum_i c_{i\alpha} c_{i\beta} c_{i\eta} f_i^{eq} \\ &\quad - \frac{\Delta t^3}{6} \nabla_\alpha \nabla_\beta \nabla_\gamma \sum_i c_{i\alpha} c_{i\beta} c_{i\gamma} c_{i\eta} (\bar{f}_i^{eq} + \tilde{f}_i^{eq}) + \frac{\Delta t^4}{24} \nabla_\alpha \nabla_\beta \nabla_\gamma \nabla_\theta \sum_i c_{i\alpha} c_{i\beta} c_{i\gamma} c_{i\theta} c_{i\eta} \bar{f}_i^{eq} \\ &\quad + \sum_i c_{i\eta} \frac{\omega_i (c_{i\alpha} c_{i\beta} - c_s^2 \delta_{\alpha\beta}) (\tau_f - 1) \tilde{\Pi}_{f,\alpha\beta}^{neq}}{2c_s^2} - \Delta t \nabla_\gamma \sum_i c_{i\gamma} c_{i\eta} \frac{\omega_i (c_{i\alpha} c_{i\beta} - c_s^2 \delta_{\alpha\beta}) (\tau_f - 1) \tilde{\Pi}_{f,\alpha\beta}^{neq}}{2c_s^2} \\ &\quad + \frac{\Delta t^2}{2} \nabla_\gamma \nabla_\theta \sum_i c_{i\gamma} c_{i\theta} c_{i\eta} \frac{\omega_i (c_{i\alpha} c_{i\beta} - c_s^2 \delta_{\alpha\beta}) (\tau_f - 1) \tilde{\Pi}_{f,\alpha\beta}^{neq}}{2c_s^2} \\ &\quad + \Delta t \sum_i c_{i\eta} F_i - \Delta t^2 \nabla_\alpha \sum_i c_{i\alpha} c_{i\eta} F_i + O(\Delta x^4), \end{aligned} \quad (27b)$$

and

$$\begin{aligned} \phi + \Delta t \partial_t \phi &= \sum_i g_i^{eq} - \Delta t \nabla_\alpha \sum_i c_{i\alpha} g_i^{eq} + \frac{\Delta t^2}{2} \nabla_\alpha \nabla_\beta \sum_i c_{i\alpha} c_{i\beta} g_i^{eq} - \frac{\Delta t^3}{2} \nabla_\alpha \nabla_\beta \nabla_\eta \sum_i c_{i,\alpha} c_{i\beta} c_{i,\eta} \bar{g}_i^{eq} \\ &\quad + \sum_i \omega_i c_{i\alpha} \left[(\tau_g - 1) \bar{\Pi}_{g,\alpha}^{neq} - \Delta t \nabla_\beta c_{i\beta} (\tau_g - 1) \bar{\Pi}_{g,\alpha}^{neq} + \frac{\Delta t^2}{2} \nabla_\beta \nabla_\eta c_{i\beta} c_{i\eta} (\tau_g - 1) \bar{\Pi}_{g,\alpha}^{neq} \right] \\ &\quad + \Delta t \sum_i G_i - \Delta t^2 \nabla_\alpha \sum_i c_{i\alpha} G_i + O(\Delta x^4), \end{aligned} \quad (28)$$

where $\tilde{\Pi}_f^{neq} = -\Delta t \rho (\nabla \mathbf{u} + \nabla \mathbf{u}^T)$ and $\bar{\Pi}_g^{neq} = -\Delta t \nabla \phi$.

According to the equilibrium distribution functions (7) and (8) for the NSEs and CDE, respectively, we can obtain the following moment conditions:

$$\begin{aligned} \sum_i f_i^{eq} &= \rho, \quad \sum_i \mathbf{c}_i f_i^{eq} = \rho \mathbf{u}, \quad \sum_i \mathbf{c}_i \mathbf{c}_i f_i^{eq} = \rho \mathbf{u} \mathbf{u} + c_s^2 \rho \mathbf{I}, \\ \sum_i \mathbf{c}_i \mathbf{c}_i \tilde{f}_i^{eq} &= c_s^2 \rho \Delta \cdot \mathbf{u}, \quad \sum_i \mathbf{c}_i \mathbf{c}_i \mathbf{c}_i \bar{f}_i^{eq} = c_s^4 \Delta \rho, \quad \sum_i F_i = 0, \quad \sum_i \mathbf{c}_i F_i = \mathbf{F}, \end{aligned} \quad (29)$$

and

$$\sum_i g_i^{eq} = \phi, \quad \sum_i \mathbf{c}_i g_i^{eq} = \phi \mathbf{u}, \quad \sum_i \mathbf{c}_i \mathbf{c}_i g_i^{eq} = c_s^2 \phi \mathbf{I}, \quad \sum_i G_i = R. \quad (30)$$

By using Eq. (29) above, one can rewrite Eq. (27) as

$$\begin{aligned} \frac{\partial \rho}{\partial t} + \nabla_\alpha (\rho u_\alpha) &= \frac{\Delta t}{2} \nabla_\alpha \nabla_\beta (\rho u_\alpha u_\beta + c_s^2 \rho \delta_{\alpha\beta}) + O(\Delta x^2), \\ \frac{\partial (\rho u_\eta)}{\partial t} &= -\nabla_\alpha (\rho u_\alpha u_\eta + c_s^2 \rho \delta_{\alpha\eta}) + \frac{\Delta t c_s^2}{2} \nabla_\alpha \nabla_\beta (\rho u_\gamma \delta_{\alpha\gamma} \delta_{\beta\eta} + \rho u_\gamma \delta_{\alpha\eta} \delta_{\beta\gamma} + \rho u_\gamma \delta_{\alpha\beta} \delta_{\gamma\eta}) \\ &\quad + \Delta t c_s^2 \nabla_\gamma \frac{(\delta_{\alpha\gamma} \delta_{\beta\eta} + \delta_{\alpha\eta} \delta_{\beta\gamma}) (\tau_f - 1) \rho (\nabla_\alpha u_\beta + \nabla_\beta u_\alpha)}{2} \\ &\quad - \frac{\Delta t^3}{6} \nabla_\alpha \nabla_\beta \nabla_\gamma (c_s^4 \Delta_{\alpha\beta\gamma\eta} \rho) + F_\eta + O(\Delta x^2). \end{aligned} \quad (31a)$$

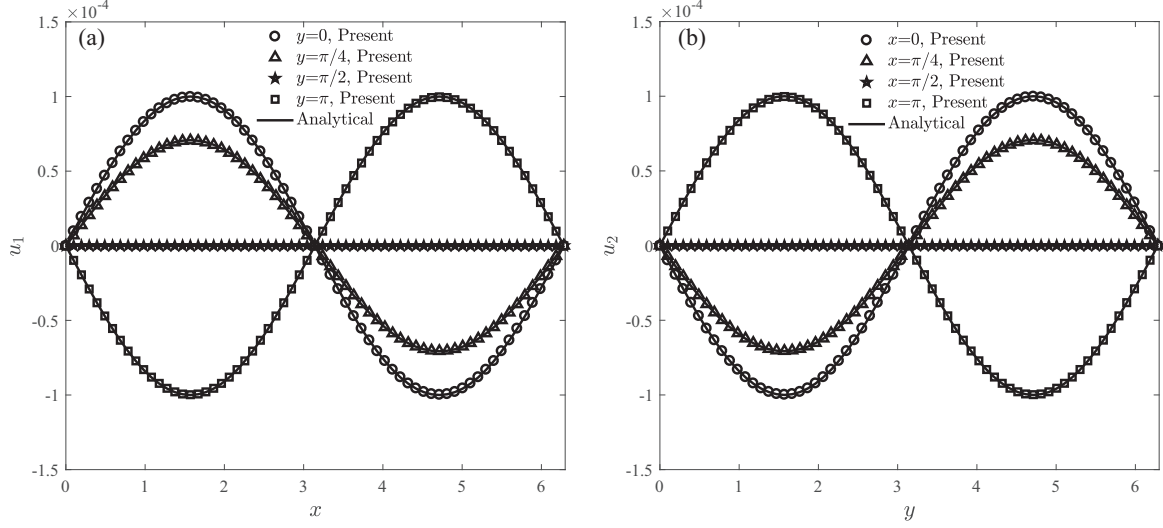


FIG. 1. The numerical and analytical solutions of velocity $\mathbf{u} = (u_1, u_2)$ at different positions [(a) u_1 and (b) u_2 . Solid line denotes the analytical solution, and symbol represents the numerical solution].

Based on the relations $p = \rho c_s^2$ and $\nabla \rho = O(Ma^2) = O(u^2/c^2) = O(\Delta x^2)$, we have

$$\frac{\partial \rho}{\partial t} + \nabla_\alpha (\rho u_\alpha) = O(\Delta x^2), \quad (32a)$$

$$\begin{aligned} \frac{\partial (\rho u_\eta)}{\partial t} + \nabla_\alpha (\rho u_\alpha u_\eta) &= -\nabla_\eta p + \nabla_\beta [\mu (\nabla_\eta u_\beta + \nabla_\beta u_\eta)] + F_\eta + \frac{\Delta t c_s^2}{2} \nabla_\eta \nabla_\beta (\rho u_\beta) + O(\Delta x^2) \\ &= -\nabla_\eta p + \nabla_\beta [\mu (\nabla_\eta u_\beta + \nabla_\beta u_\eta)] + F_\eta + O(\Delta x^2), \end{aligned}$$

where $\frac{\Delta t c_s^2}{2} \nabla_\eta \nabla_\beta (\rho u_\beta) = -\frac{\Delta t c_s^2}{2} \nabla_\eta \partial_t \rho + O(\Delta x^2) = O(\Delta x^2)$ has been used.

Similarly, with the help of Eq. (30), we can reformulate Eq. (28) as

$$\frac{\partial \phi}{\partial t} + \nabla_\alpha (\phi u_\alpha) = \nabla_\alpha D \nabla_\alpha \phi + R + O(\Delta x^2). \quad (33)$$

From above theoretical analysis, one can find that the two-level macroscopic finite-difference scheme has a second-order accuracy.

V. NUMERICAL RESULTS AND DISCUSSION

For simplicity but without the loss of generality, we only consider two-dimensional problems in this section, and three benchmark tests, including the four-roll mill problem, the isotropic CDE, and the thermal Poiseuille flow, are used to investigate the present macroscopic finite-difference schemes [(22) and (23)] in terms of the accuracy, memory usage, and computational performance. Additionally, some comparisons with the mesoscopic RLB schemes [(14) and (15)] and M-RLB schemes [(18) and (19)] are also performed. Unless otherwise stated, the D2Q9 lattice model is adopted, and all tests are carried out on the NVIDIA Tesla A100 Tensor Core equipped with 80 GB of GPU memory.

A. Four-roll mill problem

The first problem we consider is the four-roll mill problem, which has an analytical solution of the velocity \mathbf{u} , and is also a good benchmark to test the accuracy of the present scheme. In this problem, the physical domain is fixed in $[0, 2\pi] \times [0, 2\pi]$ with the periodic boundary condition imposed on all bound-

aries. To drive the fluid flow, the body force $\mathbf{F} = (F_1, F_2)$ with the following expressions are adopted:

$$\begin{aligned} F_1 &= U_0^2 \sin(x) \cos(x) + 2\nu U_0 \sin(x) \cos(y), \\ F_2 &= U_0^2 \sin(y) \cos(y) - 2\nu U_0 \sin(y) \cos(x). \end{aligned} \quad (34)$$

Then the analytical solution of the velocity $\mathbf{u} = (u_1, u_2)$ can be obtained as

$$u_1 = U_0 \sin(x) \cos(y), \quad u_2 = -U_0 \cos(x) \sin(y). \quad (35)$$

We carry out some numerical simulations with a lattice size of 64×64 , $U_0 = 0.0001$, $\nu = 0.01$, and $\Delta t = 0.2$. Figure 1 shows the numerical results with corresponding analytical solutions at different locations, and a good agreement between them can be observed. In addition, it is also known that the relaxation parameter τ_f in the LB method is a key physical parameter, and has a significant influence on the numerical stability and accuracy of the LB method. Here we give a quantitative test on the effect of relaxation time τ_f , and some simulations with the same physical parameters except for the time step Δt . To evaluate the difference between the numerical and analytical solutions, the following relative error is

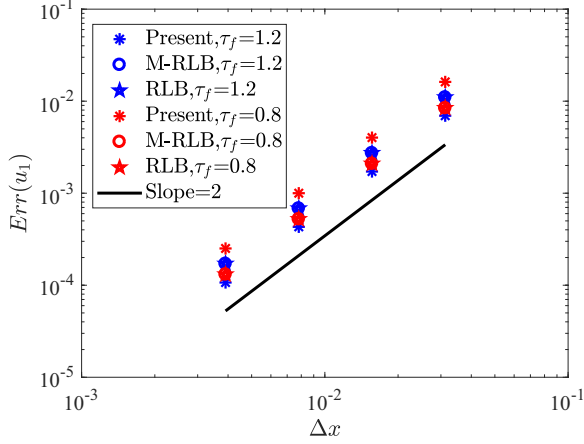


FIG. 2. A comparison of the convergence rate among the present, M-RLB, and RLB schemes for the four-roll mill problem.

adopted:

$$\text{Err} = \frac{\sum |u^n - u^a|}{\sum |u^a|}, \quad (36)$$

where the subscripts n and a represent the numerical and analytical data. The results in Table I show that when $\tau_f < 1$, the present macroscopic finite-difference scheme produces larger numerical errors than RLB and M-RLB schemes, while it gives smaller numerical errors when $\tau_f > 1$. Additionally, it is also worth noting that when $\tau_f = 1$, the relative errors of them are equal to each other since these three schemes reduce to the same one.

Theoretically, the present finite-difference scheme has a second-order convergence rate in space. To confirm this result, we now test the convergence rate numerically through changing the lattice size, and conduct a comparison with the RLB and M-RLB schemes in Fig. 2. From this figure, one can find that all three schemes have a second-order convergence rate in space, which coincide with the theoretical analysis. Besides, we also test the performance of three schemes with the lattice size 256×256 , and the simulations are suspended at the fixed iteration steps (1.5×10^5). The results in Table II indicate that, compared with the mesoscopic RLB scheme, not only the computational efficiency can be improved, but also the memory usage is less than 35%, which is highly appealing for the large-scale simulations.

B. Isotropic CDE

In this section, we adopt a simple two-dimensional isotropic CDE with a constant velocity $\mathbf{u} = (u_1, u_2)$ to test the present scheme, and the equation can be expressed as

$$\partial_t \phi + u_1 \partial_x \phi + u_2 \partial_y \phi = D(\partial_{xx} \phi + \partial_{yy} \phi) + R, \quad (37)$$

where $u_1 = u_2$, D is a diffusion coefficient defined by the Péclet number $Pe = Lu_1/D$ (L is the characteristic length and u_1 is the characteristic velocity). R is the source term, and is given by

$$R = \exp[(1 - 2D\pi^2)t] \{ \sin[\pi(x+y)] + \pi(u_1 + u_2) \cos[\pi(x+y)] \}. \quad (38)$$

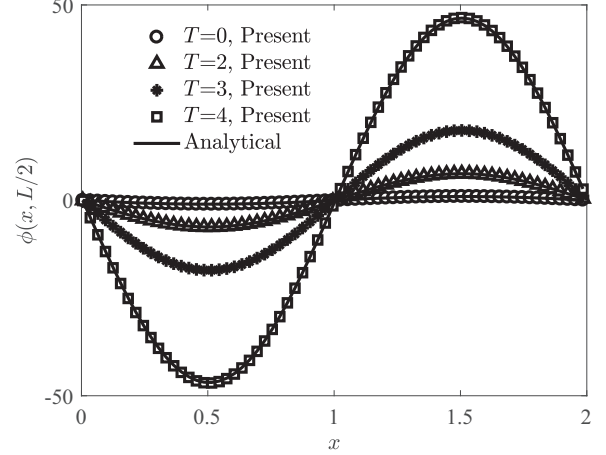


FIG. 3. The numerical and analytical solutions of ϕ at different times [solid line denotes the analytical solution, and symbol represents the numerical solution].

Under the initial condition $\phi(x, y, t = 0) = \sin[\pi(x + y)]$ and the periodic boundary condition applied on the boundaries, we can get the analytical solution as

$$\phi(x, y, t) = \exp[(1 - 2D\pi^2)t] \sin[\pi(x + y)]. \quad (39)$$

In the following simulations, the lattice size is 200×200 , $L = 2$, $Pe = 100$, $u_1 = 0.1$, and $\Delta t = 0.005$. As seen from Fig. 3, the numerical results obtained by the present scheme at different times agree well with the analytical solutions. In addition, this problem is also used to test the effect of the relaxation time τ_g . From Table III, one can obtain some similar conclusions as those shown previously. Furthermore, we focus on the convergence rate of the present finite-difference scheme. For this purpose, some simulations are performed with the lattice spacing changing from $2.0/50$ to $2.0/400$, and the results in Fig. 4 show that all three schemes have a second-order convergence rate in space, which are consistent with the theoretical analysis. Besides, we also conduct a comparison of the computational performance among different schemes with the lattice size 400×400 in Table IV, and one

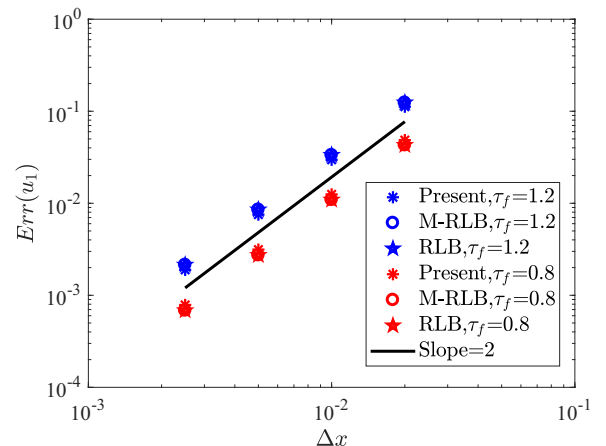


FIG. 4. A comparison of the convergence rate among the present, M-RLB, and RLB schemes for the isotropic two-dimensional CDE.

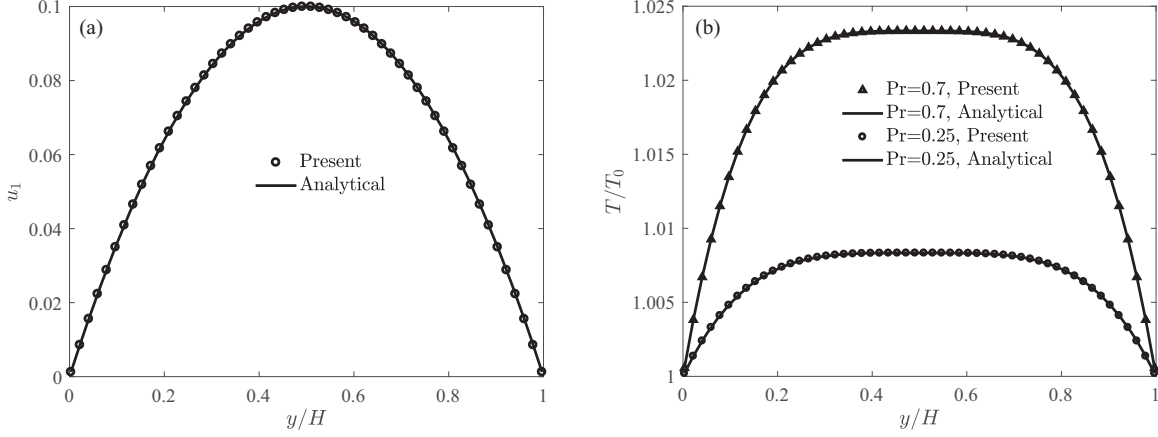


FIG. 5. The numerical and analytical solutions of (a) the velocity component u_1 and (b) the temperature field T [solid line denotes the analytical solution, and symbol represents the numerical solution].

can find that compared with the M-RLB and RLB schemes, the present scheme is not only more efficient but also has a great advantage in reducing memory occupancy.

C. Thermal Poiseuille flow

The last benchmark problem we consider is the thermal Poiseuille flow with constant wall temperature T_0 , which can be described by the following coupled equations:

$$\partial_t \rho + \nabla \cdot (\rho \mathbf{u}) = 0,$$

$$\partial_t (\rho \mathbf{u}) + \nabla \cdot (\rho \mathbf{u} \mathbf{u}) = -\nabla P + \nabla \cdot [\rho \nu (\nabla \mathbf{u} + (\nabla \mathbf{u})^T)] + \mathbf{F},$$

$$\partial_t T + \nabla \cdot (T \mathbf{u}) = \nabla \cdot (D \nabla T) + R, \quad (40)$$

where $R = 2\nu S_{\alpha\beta} S_{\alpha\beta}$ and $S_{\alpha\beta} = (\partial_\alpha u_\beta + \partial_\beta u_\alpha)/2$. In this problem, the nonslip boundary condition is applied on both bottom and top walls, and the inflow and outflow are treated by the periodic boundary condition. With the Reynolds number $Re = U_0 H / \nu$ and the Prandtl number $Pr = \nu / D$, the analytical solutions of the flow and temperature fields can be

given as [45]

$$u_1^{\text{exact}} = \frac{4Re\nu}{H} \left(\frac{y}{H} - \frac{y^2}{H^2} \right), \quad (41)$$

$$T^{\text{exact}} = T_0 + \frac{Pr U_0^2}{3} \left[1 - \left(\frac{2y}{H} - 1 \right)^4 \right],$$

where $U_0 = 0.1$ is the maximum velocity and H is the height of the channel. In our simulations $H = 1$, $T_0 = 0.1$, $Re = 0.01$, and $\mathbf{F} = (F_x, 0)$ with $F_x = 8\rho\nu U_0 / H^2$, $\Delta x = 1/80$, and $\Delta t = 2.0 \times 10^{-6}$. Figure 5 presents the comparisons of the numerical and analytical results of temperature and velocity distributions. From this figure, one can see that numerical results of both fields given by present scheme are well consistent with the analytical solutions. Moreover, we test the effect of $\tau_{f,g}$ on velocity and temperature with $Pr = 0.25$ in Table V. As seen from this table, the relative error of the velocity obtained from the present scheme is larger than those from M-RLB and RLB schemes when $\tau_f < 1$, but for all tests, the present scheme shows a better performance on the temperature. In addition, we also present the convergence rates of three schemes for velocity and temperature in Fig. 6, and it is clear that all of them have a second-order convergence rate.

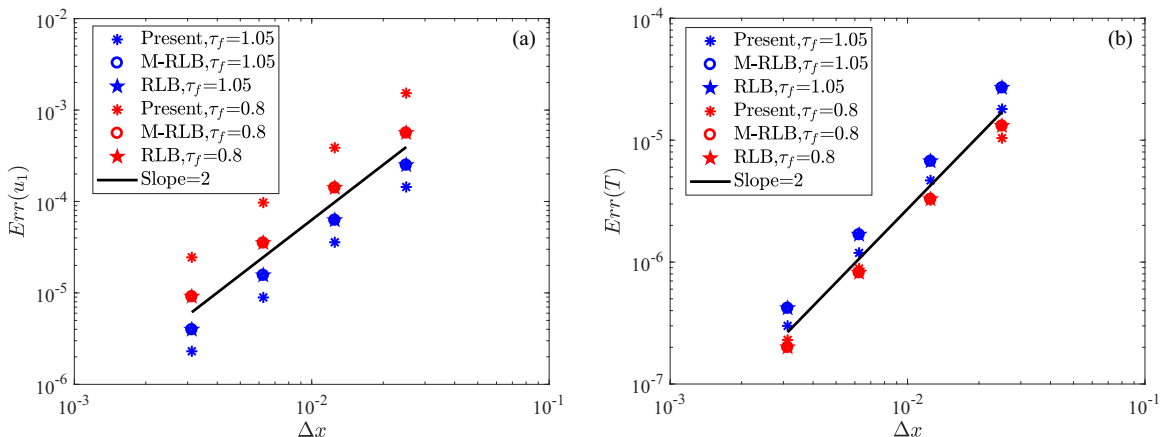


FIG. 6. A comparison of the convergence rate among the present, M-RLB, and RLB schemes for the thermal Poiseuille flow with $Pr = 0.25$ [(a) the velocity component u_1 and (b) the temperature field T].

TABLE VI. The comparisons of the memory usage and computational time among the present, M-RLB, and RLB schemes for the thermal Poiseuille flow with $Pr = 0.25$.

	Storage variables	Memory usage	Total time
Present	$\rho[NY][NX], u_1[NY][NX], u_2[NY][NX], F_x[NY][NX], T[NY][NX]$ $\tilde{\rho}[NY][NX], \tilde{u}_1[NY][NX], \tilde{u}_2[NY][NX], \tilde{T}[NY][NX]$	21.95%	10.48s
M-RLB	$\rho[NY][NX], u_1[NY][NX], u_2[NY][NX], F_x[NY][NX], T[NY][NX]$ $\tilde{\rho}[NY][NX], \tilde{u}_1[NY][NX], \tilde{u}_2[NY][NX], \tilde{T}[NY][NX]$ $\Pi_{f,xx}[NY][NX], \Pi_{f,xy}[NY][NX], \Pi_{f,yy}[NY][NX]$ $\tilde{\Pi}_{f,xx}[NY][NX], \tilde{\Pi}_{f,xy}[NY][NX], \tilde{\Pi}_{f,yy}[NY][NX]$	46.34%	12.07s
RLB	$\Pi_{g,x}[NY][NX], \Pi_{g,y}[NY][NX], \tilde{\Pi}_{g,x}[NY][NX], \tilde{\Pi}_{g,y}[NY][NX]$ $g[NY][NX][Q], \tilde{g}[NY][NX][Q], f[NY][NX][Q], \tilde{f}[NY][NX][Q]$ $\rho[NY][NX], u_1[NY][NX], u_2[NY][NX], F_x[NY][NX], T[NY][NX]$	100%	17.35s

Finally, we set $\Delta x = 1/320$ and present some results on the computational performance at a fixed number of iteration step (2.0×10^6) in Table VI, and from this figure, one can find that compared with RLB scheme, the present scheme grants nearly 78% reduction in memory usage and achieves a significant improvement in efficiency.

VI. CONCLUSION

In this paper, we developed an efficient macroscopic finite-difference scheme from the mesoscopic RLB method for NSEs and CDE. From the theoretical analysis, one can find that the same as the RLB method: this two-level macroscopic finite-difference scheme also has a second-order accuracy in space. Through simulating three benchmark problems, including the four-roll mill problem, the isotropic CDE, and the thermal Poiseuille flow, one can show that compared to the

RLB and M-RLB schemes, the present macroscopic finite-difference scheme not only has a second-order accuracy, but also shares the lowest memory requirement and highest computational efficiency. Considering the numerical accuracy and computational efficiency, in a future work we will extend the present scheme to study more complex problems, e.g., the multiphase flows and multicomponent mixtures [46–48].

ACKNOWLEDGMENTS

The computation is completed in the HPC Platform of Huazhong University of Science and Technology. This work was financially supported by the National Natural Science Foundation of China (Grants No. 12072127 and No. 51836003), the Interdisciplinary Research Program of Hust (2023JCJY002), and the Fundamental Research Funds for the Central Universities, Hust (No. 2023JYCXJJ046).

- [1] S. Chen and G. D. Doolen, Lattice Boltzmann method for fluid flows, *Annu. Rev. Fluid Mech.* **30**, 329 (1998).
- [2] S. Succi, *The Lattice Boltzmann Equation for Fluid Dynamics and Beyond* (Oxford University Press, Oxford, 2001).
- [3] Z. Guo and C. Shu, *Lattice Boltzmann Method and Its Applications in Engineering* (World Scientific Publishing Co. Pte. Ltd., Singapore, 2013).
- [4] T. Krüger, H. Kusumaatmaja, A. Kuzmin, O. Shardt, G. Silva, and E. Viggien, *The Lattice Boltzmann Method: Principles and Practice* (Springer, Switzerland, 2017).
- [5] Y. Gan, A. Xu, H. Lai, W. Li, G. Sun, and S. Succi, Discrete Boltzmann multi-scale modeling of nonequilibrium multiphase flows, *J. Fluid Mech.* **951**, A8 (2022).
- [6] D. Zhang, A. Xu, Y. Zhang, Y. Gan, and Y. Li, Discrete Boltzmann modeling of high-speed compressible flows with various depths of non-equilibrium, *Phys. Fluids* **34**, 086104 (2022).
- [7] H. Wang, X. Yuan, H. Liang, Z. Chai, and B. Shi, A brief review of the phase-field-based lattice Boltzmann method for multiphase flows, *Capillarity* **2**, 33 (2019).
- [8] H. Liu, Q. Kang, C. R. Leonardi, S. Schmieschek, A. Narváez, B. D. Jones, J. R. Williams, A. J. Valocchi, and J. Harting, Multiphase lattice Boltzmann simulations for porous media applications, *Comput. Geosci.* **20**, 777 (2016).
- [9] L. Chen, A. He, J. Zhao, Q. Kang, Z. Li, J. Carmeliet, N. Shikazono, and W. Tao, Pore-scale modeling of complex transport phenomena in porous media, *Prog. Energy Combust. Sci.* **88**, 100968 (2022).
- [10] Y. H. Qian, D. D’Humières, and P. Lallemand, Lattice BGK models for Navier-Stokes equation, *Europhys. Lett.* **17**, 479 (1992).
- [11] H. Chen, S. Chen, and W. H. Matthaeu, Recovery of the Navier-Stokes equations using a lattice-gas Boltzmann method, *Phys. Rev. A* **45**, R5339 (1992).
- [12] D. d’Humières, Generalized lattice-Boltzmann equations, in *Rarefied Gas Dynamics: Theory and Simulations*, edited by B. D. Shizgal, D. P. Weave (AIAA, Reston, VA, 1992), Vol. 159, pp. 450–458.
- [13] P. Lallemand and L.-S. Luo, Theory of the lattice Boltzmann method: Dispersion, dissipation, isotropy, Galilean invariance, and stability, *Phys. Rev. E* **61**, 6546 (2000).
- [14] Z. Chai and B. Shi, Multiple-relaxation-time lattice Boltzmann method for the Navier-Stokes and nonlinear convection-diffusion equations: Modeling, analysis, and elements, *Phys. Rev. E* **102**, 023306 (2020).
- [15] J. Latt and B. Chopard, Lattice Boltzmann method with regularized pre-collision distribution functions, *Math. Comput. Simul.* **72**, 165 (2006).

- [16] H. Chen, R. Zhang, I. Staroselsky, and M. Jhon, Recovery of full rotational invariance in lattice Boltzmann formulations for high Knudsen number flows, *Physica A* **362**, 125 (2006).
- [17] L. Wang, B. Shi, and Z. Chai, Regularized lattice Boltzmann model for a class of convection-diffusion equations, *Phys. Rev. E* **92**, 043311 (2015).
- [18] I. Ginzburg, Equilibrium-type and link-type lattice Boltzmann models for generic advection and anisotropic-dispersion equation, *Adv. Water Resour.* **28**, 1171 (2005).
- [19] I. Ginzburg, F. Verhaeghe, D. d'Humières, Two-relaxation-time lattice Boltzmann scheme: About parametrization, velocity, pressure and mixed boundary conditions, *Commun. Comput. Phys.* **3**, 427 (2008).
- [20] L. Luo, W. Liao, X. Chen, Y. Peng, and W. Zhang, Numerics of the lattice Boltzmann method: Effects of collision models on the lattice Boltzmann simulations, *Phys. Rev. E* **83**, 056710 (2011).
- [21] S. Suga, An accurate multi-level finite difference scheme for 1D diffusion equations derived from the lattice Boltzmann method, *J. Stat. Phys.* **140**, 494 (2010).
- [22] Y. Lin, N. Hong, B. Shi, and Z. Chai, Multiple-relaxation-time lattice Boltzmann model-based four-level finite-difference scheme for one-dimensional diffusion equations, *Phys. Rev. E* **104**, 015312 (2021).
- [23] G. Silva, Discrete effects on the source term for the lattice Boltzmann modelling of one-dimensional reaction-diffusion equations, *Comput. Fluids* **251**, 105735 (2023).
- [24] Y. Chen, Z. Chai, and B. Shi, Fourth-order multiple-relaxation-time lattice Boltzmann model and equivalent finite-difference scheme for one-dimensional convection-diffusion equations, *Phys. Rev. E* **107**, 055305 (2023).
- [25] Q. Li, Z. Zheng, S. Wang, and J. Liu, A multilevel finite difference scheme for one-dimensional Burgers equation derived from the lattice Boltzmann Method, *J. Appl. Math.* **2012**, 925920 (2012).
- [26] R. Fučík and R. Straka, Equivalent finite difference and partial differential equations for the lattice Boltzmann method, *Comput. Math. Appl.* **90**, 96 (2021).
- [27] R. Fučík, P. Eichler, J. Klinkovský, R. Straka, and T. Oberhuber, Lattice Boltzmann Method Analysis Tool (LBMAT), *Numer. Algorithms* **93**, 1509 (2023).
- [28] T. Bellotti, B. Graille, and M. Massot, Finite difference formulation of any lattice Boltzmann scheme, *Numer. Math.* **152**, 1 (2022).
- [29] T. Bellotti, Truncation errors and modified equations for the lattice Boltzmann method *via* the corresponding Finite Difference schemes, *ESAIM: M2AN* **57**, 1225 (2023).
- [30] M. Junk, A finite difference interpretation of the lattice Boltzmann method, *Numer. Meth. Part. Diff. Equ.* **17**, 383 (2001).
- [31] T. Inamuro, A lattice kinetic scheme for incompressible viscous flows with heat transfer, *Philos. Trans. R. Soc. London A* **360**, 477 (2002).
- [32] A. Tiribocchi, A. Montessori, G. Amati, M. Bernaschi, F. Bonaccorso, S. Orlandini, S. Succi, and M. Lauricella, Lightweight lattice Boltzmann, *J. Chem. Phys.* **158**, 104101 (2023).
- [33] Z. Chen, C. Shu, Y. Wang, L. M. Yang, and D. Tan, A simplified lattice Boltzmann method without evolution of distribution function, *Adv. Appl. Math. Mech.* **9**, 1 (2017).
- [34] S. Qin, G. Hou, L. Yang, Y. Gao, W. Guo, and J. Shi, A novel one-step simplified lattice Boltzmann method and its application to multiphase flows with large density ratio, *Phys. Fluids* **35**, 053318 (2023).
- [35] P. Kundu, I. Cohen, and D. Dowling, *Fluid Mechanics* (Elsevier, California, 2016).
- [36] T. Krüger, F. Varnik, and D. Raabe, Second-order convergence of the deviatoric stress tensor in the standard Bhatnagar-Gross-Krook lattice Boltzmann method, *Phys. Rev. E* **82**, 025701(R) (2010).
- [37] W.-A. Yong and L.-S. Luo, Accuracy of the viscous stress in the lattice Boltzmann equation with simple boundary conditions, *Phys. Rev. E* **86**, 065701(R) (2012).
- [38] Z. Chai and T. S. Zhao, Effect of the forcing term in the multiple-relaxation-time lattice Boltzmann equation on the shear stress or the strain rate tensor, *Phys. Rev. E* **86**, 016705 (2012).
- [39] H. Yoshida and M. Nagaoka, Multiple-relaxation-time lattice Boltzmann model for the convection and anisotropic diffusion equation, *J. Comput. Phys.* **229**, 7774 (2010).
- [40] Z. Chai and T. S. Zhao, Lattice Boltzmann model for the convection-diffusion equation, *Phys. Rev. E* **87**, 063309 (2013).
- [41] Z. Chai, B. Shi, and Z. Guo, A multiple-relaxation-time lattice Boltzmann model for general nonlinear anisotropic convection-diffusion equations, *J. Sci. Comput.* **69**, 355 (2016).
- [42] A. Kumar, Isotropic finite-differences, *J. Comput. Phys.* **201**, 109 (2004).
- [43] X. Liu, Z. Chai, C. Zhan, B. Shi, and W. Zhang, A diffuse-domain phase-field lattice Boltzmann method for two-phase flows in complex geometries, *Multiscale Model. Simul.* **20**, 1411 (2022).
- [44] X. Liu, Z. Chai, and B. Shi, Improved hybrid Allen-Cahn phase-field-based lattice Boltzmann method for incompressible two-phase flows, *Phys. Rev. E* **107**, 035308 (2023).
- [45] H.-C. Mai, K.-H. Lin, C.-H. Yang, and C.-A. Lin, A thermal lattice Boltzmann model for flows with viscous heat dissipation, *Comput. Model. Eng. Sci.* **61**, 45 (2010).
- [46] S. Mao, D. Kuldinow, M. P. Haataja, and A. Košmrlj, Phase behavior and morphology of multicomponent liquid mixtures, *Soft Matter* **15**, 1297 (2019).
- [47] L. N. Carenza, G. Gonnella, A. Lamura, D. Marenduzzo, G. Negro, and A. Tiribocchi, Soft channel formation and symmetry breaking in exotic active emulsions, *Sci. Rep.* **10**, 15936 (2020).
- [48] G. Negro, L. N. Carenza, G. Gonnella, F. Mackay, A. Morozov, and D. Marenduzzo, Yield-stress transition in suspensions of deformable droplets, *Sci. Adv.* **9**, ead8106 (2023).